Colloidosome-Templated Poly (L-lactic acid) Crystalsomes

Mark C. Staub, Shichen Yu, and Christopher Y. Li\*

Department of Materials Science and Engineering, Drexel University, Philadelphia,

Pennsylvania, 19104 United States

\* Correspondence to: chrisli@drexel.edu

**Keywords:** Polymer crystallization, polymer single crystals, crystalsomes, colloidosomes,

spherical crystallography, poly(L-lactic acid)

Abstract

Polymers have been utilized to direct nanoparticle (NP) assembly into complex shapes and

morphologies. Strategies for polymer-directed NP assembly often involve tuning the phase

behavior of multi-component polymer/nanoparticle systems. In this work, we report the co-

assembly of polymer and NPs into hollow vesicles using confined polymer crystallization-directed

assembly. 5 nm and 20 nm Fe<sub>3</sub>O<sub>4</sub> NPs are used as the solid surfactants to create Pickering

emulsions of water and poly(L-lactic acid) (PLLA) toluene solution. The oil/water interface of the

emulsion droplets templates the growth of PLLA crystals, which in turn, immobilize NPs onto the

crystal surface, leading to the formation of colloido-polymer-crystalsomes (CPCs). The structure,

morphology, and formation mechanism of the CPCs are investigated using electron microscopy

and thermal analysis techniques. This work provides a new approach to fabricate nanoscale

complex NP-polymer conjugates.

1

## Introduction

Nanoparticles (NPs), both dispersed in solution and assembled in the solid state, have demonstrated intriguing optical, electronic, and mechanical properties. [1-5] Of particular interest is assembling NPs to desired structures for various applications. [6-19] Surfactants and polymers have been used to direct NPs to assemble into complex morphologies and structures. [18] Structure formation in this regard is largely driven by co-assembly of polymer/NPs to achieve a global free energy minimum, which often involves the redistribution of polymer ligands on the NP surfaces. [20] Spherical NP vesicles have been attained using this approach. For example, It was shown that gold nanoparticles (AuNPs) tethered with poly(ethylene oxide) (PEO) and poly(methyl methacrylate) (PMMA) can self-assemble into vesicle structure with the AuNPs embedded in the PMMA layer. [21] Hybrid Janus vesicles were prepared by co-assembly of hydrophobic Fe<sub>3</sub>O<sub>4</sub> NPs, free amphiphilic block copolymers (BCPs), and AuNP coated with the BCP. [22] Both spherical and hemispherical shapes of the assembly were observed. [22] Fe<sub>3</sub>O<sub>4</sub> NPs were also incorporated into polymersomes formed by the self-assembly of poly(acrylic acid) (PAA)-b-poly (styrene) (PS) amphiphilic block copolymers (BCPs). [23]

Another intriguing spherical NP assembly structure is the so-called colloidosome, which is formed by pinning NPs or microparticles at the water/oil interface of an emulsion.[24-28] These NPs serve as the solid-state surfactants to stabilize the emulsion.[24-28] The interstitial space between adjacent NPs provides a means for selective diffusion of molecules or drugs. To harvest colloidosomes for various application purposes, the colloidal particles at the emulsion surface are "crosslinked" using methods including infusion of NPs, crosslinking of ligands surrounding the NPs, and polyelectrolyte complexation.[28] Polymer single crystals (PSCs) have been utilized to template NP assembly.[29-33] Typically formed by folding polymer chains into quasi-two

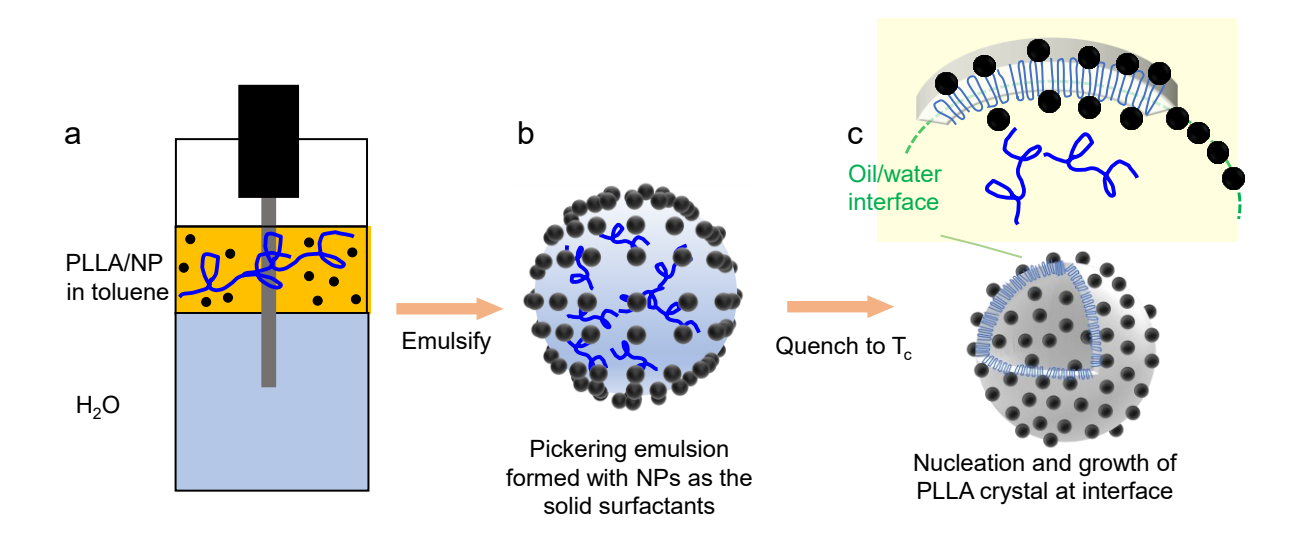
dimensional (2D) nanometer-thin sheets, PSCs can then immobilize NPs on their surface, leading to co-assembly of polymer and NPs.[30] Flat 2D and linear 1D NP assemblies templated by PSCs have been reported, [29, 34, 35] and these unique free-standing NP/PSC conjugates have found applications in nanoparticle synthesis, [36] artificial nanomotors, [37] surface enhanced Raman spectroscopy,[38] directing ion transport, etc.[39] On the other hand, spherical polymer crystalsome structures have been recently reported.[40-46] The morphology of crystalsomes is quite similar to the previous reported colloidosomes – both are spherical, nanosized hollow particles and can be formed in miniemulsion systems. Moreover, nucleation and growth of polymer crystals from nanofillers at liquid/liquid interface has also been studied.[47, 48] These studies motivated us to investigate the feasibility of co-assembling NPs and PSCs in a miniemulsion system. In this work, an Fe<sub>3</sub>O<sub>4</sub> NP-stabilized miniemulsion is used to template the formation of poly(L-lactic acid) (PLLA) crystalsomes. Hollow particles comprised of PSCs and NPs are formed. The solid 2D PSCs provide another means to immobilize NP assembly in colloidosomelike templates. Because of the nucleation—growth nature of the crystalsome formation mechanism, intermediate states of the assemblies with open shell structure can be captured. Our work demonstrates a new approach to achieve controlled assembly of NPs with vesicle-like and nonconventional morphologies.

## **Results and Discussion**

## Polymer crystallization in nanoparticle-stabilized emulsions

**Scheme 1** shows the fabrication strategy employed to investigate polymer crystallization templated by NP-stabilized emulsions. Briefly, PLLA homopolymer is dissolved in an Fe<sub>3</sub>O<sub>4</sub> NP toluene solution (5 mg/mL) at 105 °C (**Scheme 1a**) and then mixed with DI H<sub>2</sub>O which is pre-

heated at the same temperature. The miniemulsion is then generated via probe sonication of the mixture using the NPs as the solid surfactants (**Scheme 1b**). Note that the NPs are pinned at the emulsion interface due to the lowered overall free energy of the system, the Pickering mechanism, and the PLLA polymer is dissolved in the emulsion droplet. The system is then brought to 70 °C for crystallization. The formed PLLA nuclei are also anticipated to be pinned at the oil/water interface, similar to the previously reported crystalsome cases. As it grows, the PSC expels the NPs from the growth front and the NPs are immobilized on the crystal surface, as shown in **Scheme 1c**.



**Scheme 1.** The formation process of colloido-polymer-crystalsomes. (a) H<sub>2</sub>O and PLLA/NP toluene solution are used as the water/oil phase, respectively. (b) A miniemulsion droplet stabilized by NPs and the polymers are dissolved inside the droplet. (c) Crystallization of PLLA leads to the colloido-polymer-crystalsome particles.

Figure 1 shows a typical scanning electron microscopy (SEM) image of the polymer crystals prepared using the 5 nm NP colloidosome templates after 2-days of crystallization. The crystal is non-flat and three-dimensional (3D), which is consistent with the previously reported crystalsomes.[40] The size of the particles ranges from hundreds of nm to several µm. Polymer layered lamellae can be seen on the surface of the particles, blue arrow, in **Figure 1b**. Interestingly, multiple tie chains (red arrows) can also be seen connecting two lamellar surfaces, suggesting that multilayered structures can form and there are connected via polymer chains between the adjacent lamellae.[33] The particles are not quite spherical, instead, they appear polyhedron-like with quite distinct facets which is different from the previously reported PLLA crystalsomes templated by small molar mass surfactants.[40] Figures 1b-d are three crystals obtained using the same method and the morphology resembles a crystal viewed from different directions, further confirming the non-spherical morphology of the crystal. It is evident from Figure 1d that these particles are hollow capsules and are not completely closed, even in some areas there is overlapping of polymer lamellae. The small opening area (green arrow in Figure 1d) indicates that the polymer crystals stopped growth before they can completely cover the emulsion droplet surface, which again is different from the previous PLLA crystalsomes.[40] The openness of the structure could be attributed to the lack of polymers in the solution and nanoparticle surfactants. The multiple-faceted nature can be associated with lamellar growth, which will be discussed later. Because these capsules are comprised of both NPs and PSCs, colloido-polymer-crystalsomes (CPCs) will be the naming convention used in the following discussion of this unique structure.

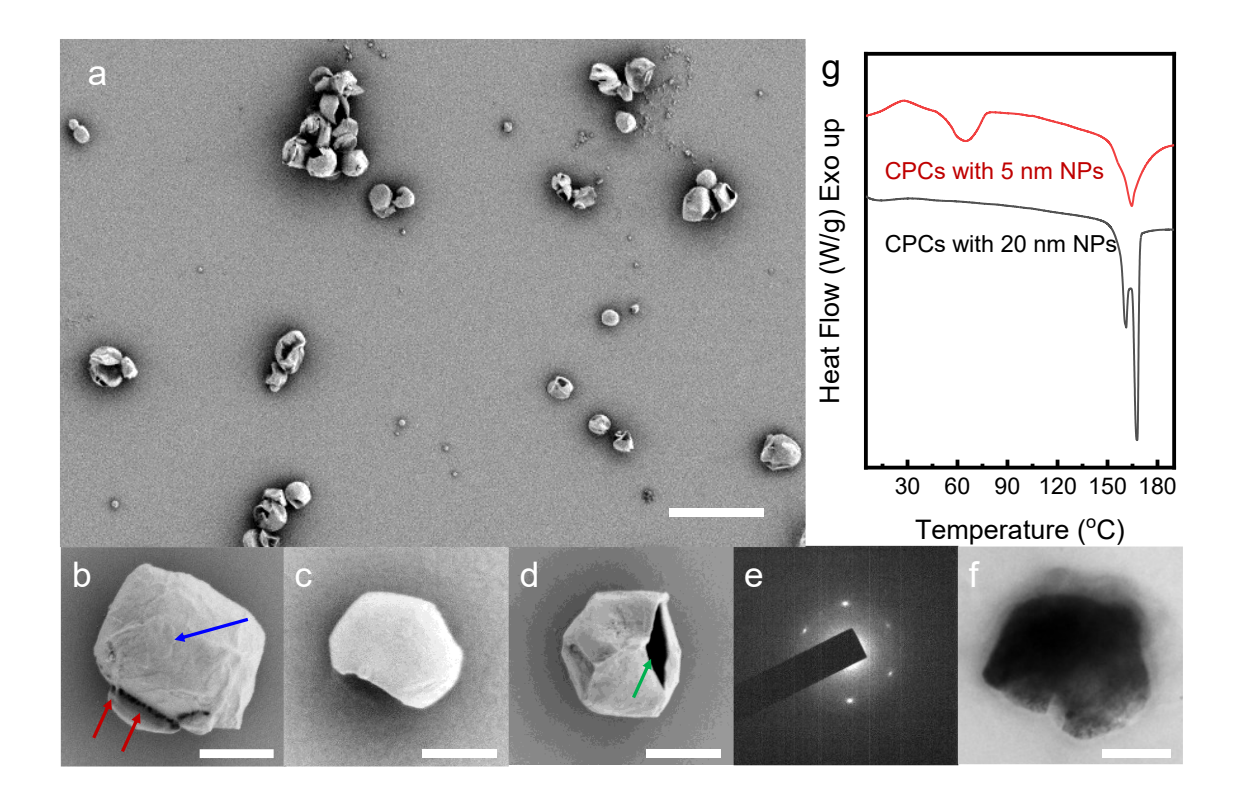


**Figure 1**. PLLA colloido-polymer-crystalsomes. (a-d) SEM images of PLLA CPCs comprised of 5 nm NP and PLLA PSCs at different magnifications. (b-d) reveal polyderon-like shapes of the CPCs. (e) SAED pattern of a PLLA CPC containing 5 nm NPs and (f) the corresponding bright field TEM image. (g) DSC first heating thermograms of CPCs formed by PLLA and 5 nm (red) / 20 nm (black) NPs. Scale bars in (a)  $10 \mu m$ , (b-d)  $1 \mu m$ , and (f) 400 nm.

To confirm the crystalline nature of these CPCs, selected area electron diffraction (SAED) experiments were conducted. **Figure 1e** shows a representative SAED pattern and **Figure 1f** is the corresponding bright field image. The SAED pattern is consistent with an [001] zone diffraction for α-phase PLLA with (200) and (110) diffraction spots.[40, 49, 50] The bright field image shows quite dark appearance, which is due to the high contrast associated with NPs. Clearer images of the NPs will be presented later. Differential scanning calorimetry (DSC) was used to examine the

thermal properties of the CPCs. The red curve in Figure 1h shows the first heating DSC trace of CPCs formed by 5 nm NPs and PLLA lamellae. A broad glass transition (Tg) with accompanying hysteresis peak at 64.3 °C and a melting point (T<sub>m</sub>) of 164.6 °C can be seen, and the percent crystallinity is ~ 25 % using a heat of fusion of 91 J/g for 100% crystalline samples of PLLA.[44] Compared to previously reported PLLA crystalsomes, CPCs show similar  $T_m$ . However, two main differences can be identified: 1) there is a clear hysteresis peak (enthalpy relaxation) in the glass transition region in CPCs while this peak is absent in PLLA crystalsomes; [44] 2) CPCs show lower crystallinity (25% vs 50-60% in 300-400 nm PLLA crystalsomes).[44] We attribute both differences to the NP effect: NPs are trapped in the vicinity of the PLLA lamellar fold surface, which reduces its order, and hinders its relaxation during heating. To confirm this, CPCs using 20 nm Fe<sub>3</sub>O<sub>4</sub> NPs and PLLA PSCs were also prepared. The DSC heating trace (black curve in Figure 1g) shows multiple melting peaks at 161.2 and 167.6 °C but no clear T<sub>g</sub>. The percent crystallinity is  $\sim 32$  %. The absence of a clear  $T_g$  and the presence of multiple melting are more common to PLLA single crystals.[44] This suggests that the relatively large 20 nm NPs are likely more excluded from the fold surface of the PSCs, and therefore the DSC heating thermogram closely mimics that of a pure PSC crystalsome. [44] Also note that recrystallization during heating is absent in both CPCs, while it was observed in pure PLLA crystalsomes, suggesting that NPs do hinder chain rearrangement for cold crystallization.

To better view the NPs on the surface of a CPC, high magnification TEM imaging was used, and the results are shown in **Figure 2**. **Figure 2a** is a relatively spherical CPC fabricated with 5 nm NPs and having a diameter of ~ 460 nm. Fe<sub>3</sub>O<sub>4</sub> NPs are clearly seen, covering nearly the entire surface of the CPC. The hydroxy group chain ends and the ester group in PLLA could facilitate PSC-NP adhesion.[37] The NPs also appear to be tightly packed, showing different

packing symmetries in different locations of the CPC. For example, the NPs in the left domain (red circle) have a hexagonal symmetry, while in the central lower region, the packing appears to be square (blue circle). In the upper central region (white circle), the packing symmetry is unclear with particles seeming to form chains. The appearance of different packing symmetries on one CPC is presumably because 1) the local packing of the NPs could vary due to the dynamic nature of the oil/water surface and the NP immobilization process, and 2) in different regions on the curved surface of the sphere, the NP assemblies are projected on the recording screen at different angles. In another example, TEM tilting experiments were conducted on a small CPC and Figure **2b-d** shows the CPC without tilting (**Figure 2b**) and after tilting for  $\pm 30^{\circ}$  (**Figures 2c,d**, also see supporting Figure S1). The packing symmetry apparently changes as the viewing angle changes. It is intriguing that the NP packing shows well-ordered packing in CPCs. In our previous work using pre-formed PSCs to immobilize NPs, NPs are poorly ordered on the surface of PSCs because of the rough PSC surfaces. [29, 34] In the present case, good packing order of the NPs suggests that NPs first packed in an ordered fashion at the liquid/liquid interface before polymer crystallization, and "small domains of 2D NP assemblies" such as those in the dotted circles in Figure 2a likely adhere to the PSC surface together and the original packing order is therefore not significantly distorted during the crystallization/immobilization process.

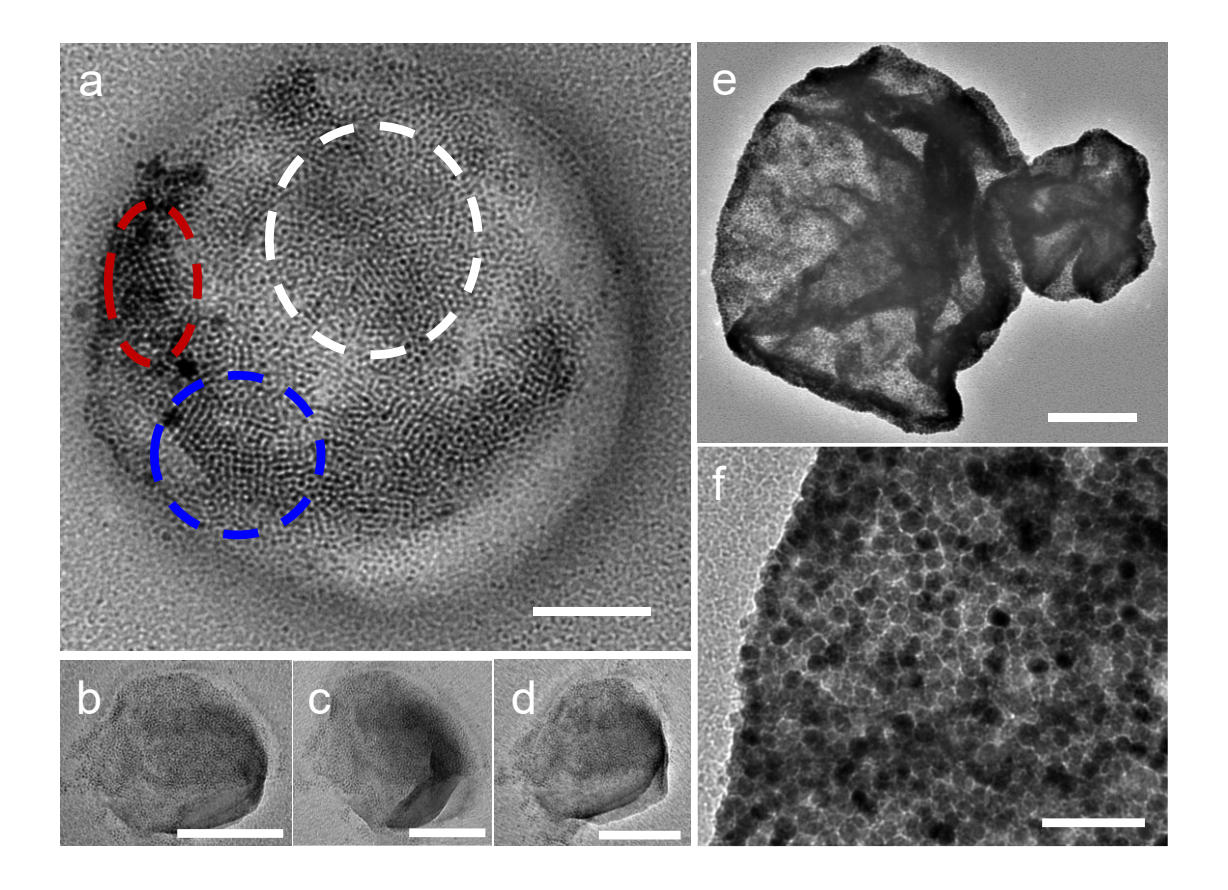


**Figure 2.** NPs on CPCs. (a) TEM bright field image of a CPC comprised of 5 nm NP and PLLA PSCs. Circles with different colors highlight different packing symmetries of the NPs. (b-d) show TEM bright field images of a CPC with 0, 30, and -30 degrees of tilting, respectively. (e) is a TEM image of a CPC comprised of 20 nm NP and PLLA PSCs, and (f) is an enlarged image of (e). In (e, f), NPs are closely packed while the packing symmetry is unclear. Scale bars in (a, f) 100 nm and in (b-e) 200 nm.

**Figure 2e** shows the TEM image of CPCs formed by 20 nm NPs and PLLA PSCs. The edges of the CPCs are relatively rough and non-spherical. NPs can be clearly seen and **Figure 2f** shows the enlarged image of **Figure 2e**. The NPs are closely packed. However, unlike in the case of 5nm NP CPCs, the packing symmetry of the NPs in **Figures 2** is unclear. Considering a particle

with a radius r and two liquid phases (phase 1 and 2), the decrease of the total free energy of the particles from one phase to the liquid/liquid interface of 1 and 2 can be described as  $\Delta E = \frac{\pi r^2}{\gamma_{21}} \cdot [\gamma_{21} - |\gamma_{P2} - \gamma_{P1}|]^2 \cdot [24]$  The three contributions to the interfacial energy arise from the particle/phase 1 interface ( $\gamma_{P1}$ ), the particle/phase 2 interface ( $\gamma_{P2}$ ), and the phase 1/phase 2 interface  $(\gamma_{21})$ . For a given emulsion system (i.e. with fixed  $\gamma_{P1}$ ,  $\gamma_{P2}$ , and  $\gamma_{21}$ ), the stability of the nanoparticle assembly is determined by the square of the NP radius r. In the present case, the emulsion formed by 20 nm NPs, provides a much more stable interface, the morphology shown in Figures 2 e,f therefore reflect the NP ordering in the emulsion state. The lesser ordering can be attributed to the large particle size. When considering particles crystallization at a spherical liquid/liquid interface, the ratio between the NP and emulsion radius, r and R, respectively, is important.[51] A small r/R means that the particle does not experience the curvature effect when packing at the interface. As r/R increases, the NPs "feel" the curvature of the interface, leading to increasingly frustrated NP packing. Furthermore since it is energetically more costly to displace larger NPs (20 nm) into liquid phases, NPs are more likely jammed at the interface with less ordered packing, which could contribute to the formation of non-spherical polyhedron shapes. Furthermore, it also manifests itself in the PSC morphology development. The CPC shells are formed by NP-decorated PLLA lamellae, which are anticipated to be stiffer compared with PLLA lamellae, leading to the deviation of spherical shapes.

## CPC morphology evolution at the liquid/liquid interface

To understand how the non-spherical morphologies of CPC polyhedrons are formed, early time points were taken for SEM analysis. **Figure 3** shows the CPCs formed after 10 min~ 3 hrs of

growth. Because of the sporadic nucleation of the crystals, different stages of the crystal growth can be observed. The morphology observed after 10 min of growth show that some of the curved crystals are already formed. The crystal is similar to the classical lozenge-shaped, flat 2D PLLA lamella, but is curved along the white arrow in **Figure 3a**. In other cases, half spherical shells can be seen (**Figure 3b**), suggesting that the aspect ratio of the crystals vary. More interestingly, at the 3-hour time-point, some crystals begin to grow anisotropically: along the long axis of the crystal, accelerated growth in this direction led to the formation of a protrusion (green arrow in **Figure 3c**) and the orthogonal growth appears to be slower. There also appears to be a reentry region of the crystal (white arrow in **Figure 3c**), which likely results from the accelerated growth of the protrusion.

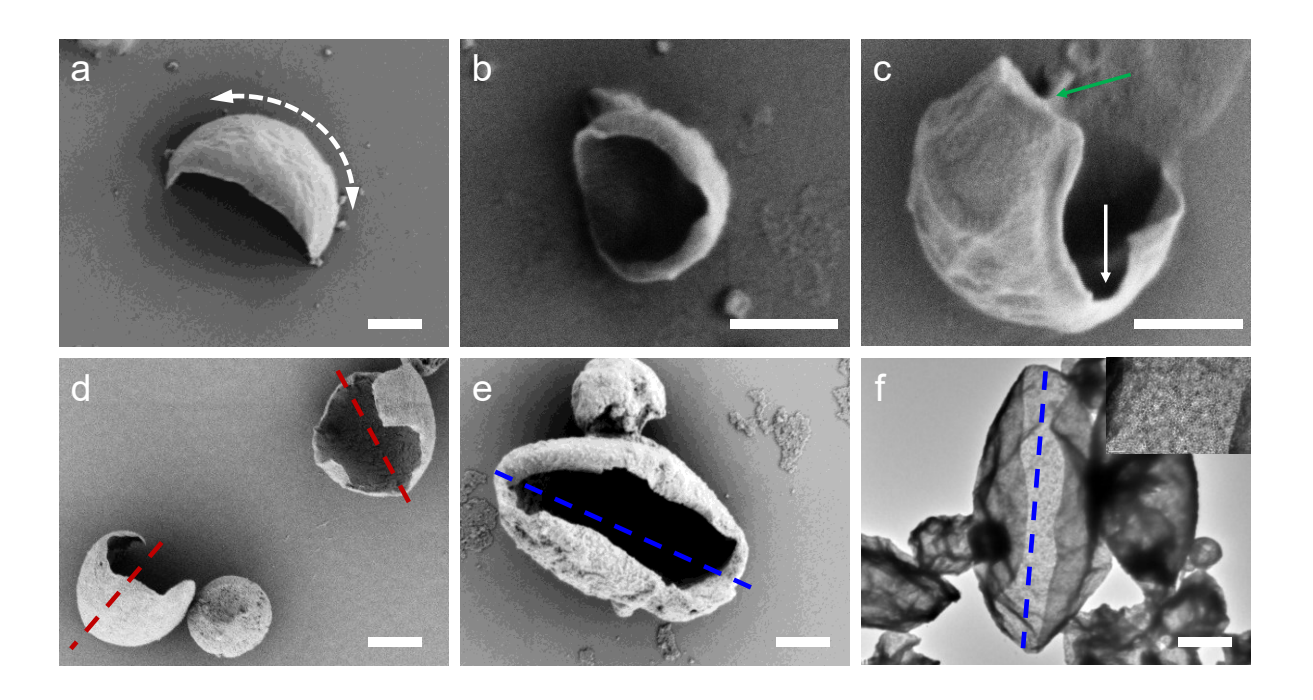


**Figure 3.** Evolution of CPCs. SEM images of different stages of 5 nm NP CPCs (a-c) and 20 nm NP CPCs (d and e). The crystal bends along the short axis (red lines) in (d) and the long axis in

(e). (f) shows TEM image of ellipsoidal CPCs. Inset is the enlarged central domain of the CPC. Scale bars in (a, d-f) 1 μm and in (b-c) 500 nm.

This switch in growth habit from relatively isotropic to anisotropic (protrusion in Figure **3c**) on curved surfaces has been observed in particles packed on spherical droplets.[51] Bending of a narrower ribbon on a curved surface would be energetically less costly compared with deforming a wider ribbon.[51] A similar growth process was also observed in the case of 20 nm CPCs. Figure 3d shows an SEM image capturing the "protrusion" of PLLA lamellae similar to Figure 3c. The protrusion in Figure 3d is more advanced, and the original (110) plane of PLLA PSC disappeared due to the formation and propagation of the protrusion parallel to the [100] axis direction. These morphological markers of underlying structural translations come from consideration of a 2D lozenge PLLA PSC where the long axis is the a-direction. Interestingly, we also occasionally observed ellipsoidal CPCs when 20 nm NPs were utilized as shown in Figures **3e,f.** In this case, PSC bend along the long axis (blue dashed line) of the crystal, leading to an oblong shaped capsule. This suggests that the free energy difference (elastic energy of bending) along these two axes are similar and both cases were observed. The absence of these ellipsoidal CPCs in 5 nm CPCs is likely due to the NP size effect: in the 5 nm NP CPC cases, PSC dominates the system since NPs are small, and therefore the bending along the short axis of the crystal manifest itself in the morphological development. In the 20 nm CPCs, since the NP size is greater than the PSC thickness (~ 10 nm), the NP layer therefore dictate the bending direction, which diminishes the difference of the anisotropy of PSC growth.

## Crystalsome with closed shell with CTAB co-surfactant

The above experiments demonstrate that CPCs are formed using colloidal particles as the solid surfactants for emulsification. They are, however, not completely closed as shown in **Figure 1**. From an application standpoint, it is of interest to seek a closed shell structure. To study this, the miniemulsion system was modified to incorporate 0.2 wt.% cetrimonium bromide (CTAB) as a co-surfactant. **Figures 4a,b** show SEM and TEM images, respectively, of the 5 nm NP CPC system (lower magnification SEM images shown in Figure S.2). The CPCs in this case appear closed with what seems like NP or NP aggregation on the CPC surface. The previously observed facets and polyhedron structure are no longer present. TEM imaging reveals that the NPs are all located on one side of the CPCs, leading to a Janus type structure. The inclusion of co-surfactant therefore stabilizes the droplet before PLLA crystallization, NPs are also likely enriched on one side of the droplet, leading to the observed Janus CPCs. This was absent in the previous CPCs, since NPs are necessary to cover the entire surface of the emulsion droplets to stabilize the latter.

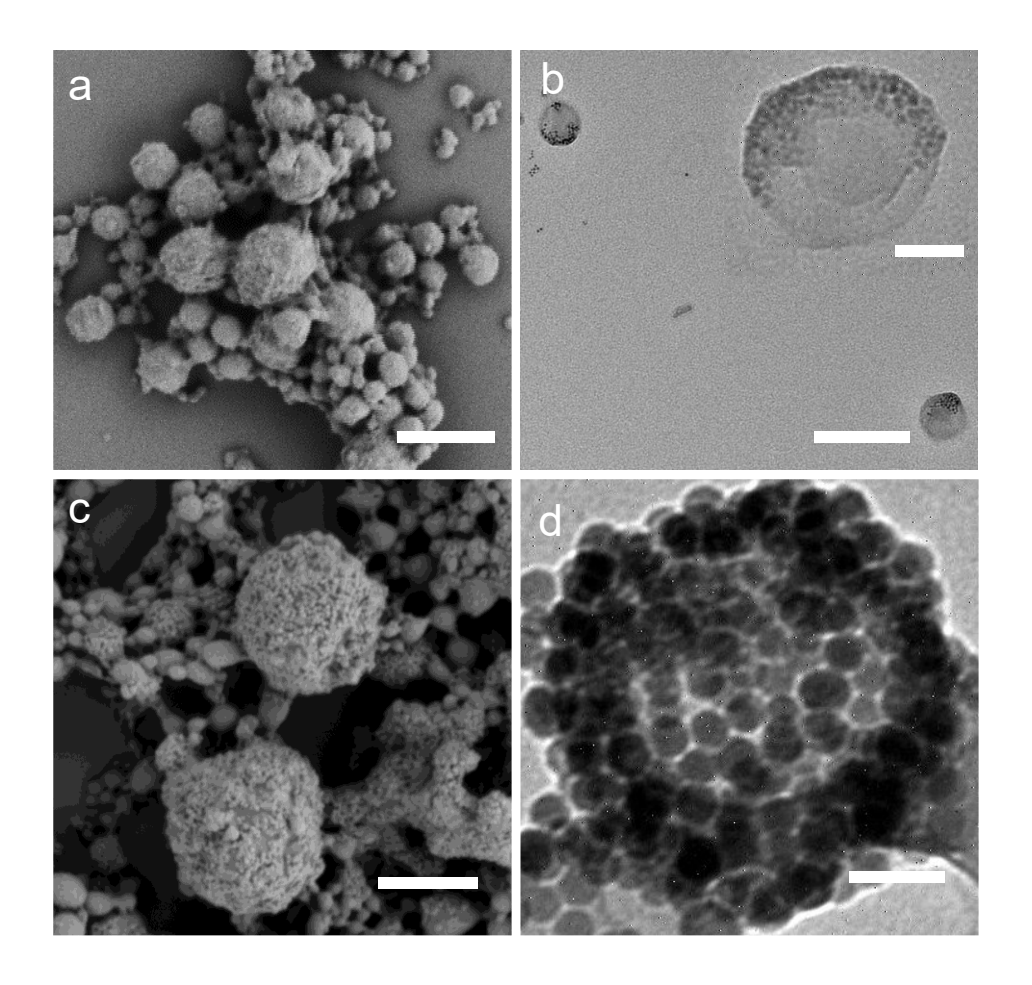


**Figure 4.** CPCs formed by using NP and co-surfactant. (a-b) SEM (a) and TEM (b) images of 5 nm NP CPCs with 0.2 wt% CTAB added to the system. (c-d) SEM (c) and TEM (d) images of 20 nm NP CPCs with 0.2 wt% CTAB added to the system. Scale bars in (a, c) 500 nm, in (b) 200 nm, and in (b inset, d) 40 nm.

**Figures 4c,d** show the SEM and TEM images of the 20 nm NP CPCs. In this case the SEM image shows that the CPCs are spherical and have a rough surface decorated with many particles on the surface matching the size expected for 20 nm NPs. Looking further into the TEM, it is observed the NPs are located homogenously around the entire shell surface and the Janus feature in the 5nm NP CPCs is not observed, suggesting that phase separation between NPs and CTAB

didn't occur in the 20 nm NP emulsion. Another feature is the difference in electron contrast in the middle and sides of the shell. If the high Z number NPs were in the shell at a significant amount, then a similar contrast though the entire crystalsome would be observed. Detailed understanding of the NP/polymer/co-surfactants phase separation and NP location in the polymer crystallization process certainly warrant further investigation.

## **Conclusion**

A one-pot fabrication strategy was developed to form co-assemblies of PLLA crystals and Fe<sub>3</sub>O<sub>4</sub> NPs in a miniemulsion system named as CPCs. When either 5 nm or 20 nm NPs were used as the lone surfactant to produce the emulsion, the resultant CPCs showed a polyhedron shape with different degrees of openings. This was attributed to the fact that once NPs are attached to the surface of crystals, which are locally flat and globally curved, the smooth curvature driven by minimizing the surface free energy is overwhelmed by the local NP and crystal packing. It was shown that crystal growth habit is affected by the curvature of the droplet, and sharp protrusions of the crystal are formed at the late stage of the CPC formation. Thermal analysis suggested that 5nm NPs are more intricately bound on the lamellar surface, leading to lower crystallinity, while larger 20nm NPs are readily expelled from the lamellae. It was also demonstrated that introducing small molar mass co-surfactants led to spherical and closed CPCs. We anticipate that this method provides another means to achieve spherical NP assembly with tunable morphologies.

# **Acknowledgement:**

This research was financially supported by the National Science Foundation DMR 2104968 and DMR 1709136.

#### **References:**

- [1] A.P. Alivisatos, Semiconductor clusters, nanocrystals, and quantum dots, Science 271 (1996) 933-937.
- [2] C.B. Murray, C.R. Kagan, M.G. Bawendi, Synthesis and characterization of monodisperse nanocrystals and close-packed nanocrystal assemblies, Annu. Rev. Mater. Sci. 30 (2000) 545-610.
- [3] M.C. Daniel, D. Astruc, Gold nanoparticles: Assembly, supramolecular chemistry, quantum-size-related properties, and applications toward biology, catalysis, and nanotechnology, Chem. Rev. 104 (2004) 293-346.
- [4] D.V. Talapin, J.-S. Lee, M.V. Kovalenko, E.V. Shevchenko, Prospects of colloidal nanocrystals for electronic and optoelectronic applications, Chem. Rev. 110 (2010) 389-458.
- [5] K. Saha, S.S. Agasti, C. Kim, X. Li, V.M. Rotello, Gold nanoparticles in chemical and biological sensing, Chem. Rev. 112 (2012) 2739-2779.
- [6] M.R. Bockstaller, R.A. Mickiewicz, E.L. Thomas, Block copolymer nanocomposites: Perspectives for tailored functional materials, Adv. Mater. 17 (2005) 1331-1349.
- [7] A.C. Balazs, T. Emrick, T.P. Russell, Nanoparticle polymer composites: Where two small worlds meet, Science 314 (2006) 1107-1110.
- [8] S. Srivastava, N.A. Kotov, Nanoparticle assembly for 1D and 2D ordered structures, Soft Matter 5 (2009) 1146-1156.

- [9] L. Xu, W. Ma, L. Wang, C. Xu, H. Kuang, N.A. Kotov, Nanoparticle assemblies: dimensional transformation of nanomaterials and scalability, Chem. Soc. Rev. 42 (2013) 3114-3126.
- [10] T. Wang, D. LaMontagne, J. Lynch, J. Zhuang, Y.C. Cao, Colloidal superparticles from nanoparticle assembly, Chem. Soc. Rev. 42 (2013) 2804-2823.
- [11] L. Wang, L. Xu, H. Kuang, C. Xu, N.A. Kotov, Dynamic Nanoparticle Assemblies, Acc. Chem. Res. 45 (2012) 1916-1926.
- [12] Z. Lu, Y. Yin, Colloidal nanoparticle clusters: functional materials by design, Chem. Soc. Rev. 41 (2012) 6874-6887.
- [13] S.V. Kershaw, A.S. Susha, A.L. Rogach, Narrow bandgap colloidal metal chalcogenide quantum dots: synthetic methods, heterostructures, assemblies, electronic and infrared optical properties, Chem. Soc. Rev. 42 (2013) 3033-3087.
- [14] J. Kao, K. Thorkelsson, P. Bai, B.J. Rancatore, T. Xu, Toward functional nanocomposites: taking the best of nanoparticles, polymers, and small molecules, Chem. Soc. Rev. 42 (2013) 2654-2678.
- [15] B. Gao, M.J. Rozin, A.R. Tao, Plasmonic nanocomposites: polymer-guided strategies for assembling metal nanoparticles, Nanoscale 5 (2013) 5677-5691.
- [16] M.A. Boles, M. Engel, D.V. Talapin, Self-assembly of colloidal nanocrystals: From intricate structures to functional materials, Chem. Rev. 116 (2016) 11220-11289.
- [17] H. Duan, Y. Yang, Y. Zhang, C. Yi, Z. Nie, J. He, What is next in polymer-grafted plasmonic nanoparticles?, Giant 4 (2020) 100033.
- [18] C. Yi, Y. Yang, B. Liu, J. He, Z. Nie, Polymer-guided assembly of inorganic nanoparticles, Chem. Soc. Rev. 49 (2020) 465-508.
- [19] Z. Cai, Z. Li, S. Ravaine, M. He, Y. Song, Y. Yin, H. Zheng, J. Teng, A. Zhang, From colloidal particles to photonic crystals: advances in self-assembly and their emerging applications, Chem. Soc. Rev. 50 (2021) 5898-5951.
- [20] C. Yi, H. Liu, S. Zhang, Y. Yang, Y. Zhang, Z. Lu, E. Kumacheva, Z. Nie, Self-limiting directional nanoparticle bonding governed by reaction stoichiometry, Science 369 (2020) 1369-1374.

- [21] J. Song, L. Cheng, A. Liu, J. Yin, M. Kuang, H. Duan, Plasmonic vesicles of amphiphilic gold nanocrystals: self-assembly and external-stimuli-triggered destruction, J. Am. Chem. Soc. 133 (2011) 10760-10763.
- [22] Y. Liu, X. Yang, Z. Huang, P. Huang, Y. Zhang, L. Deng, Z. Wang, Z. Zhou, Y. Liu, H. Kalish, Magneto-plasmonic janus vesicles for magnetic field-enhanced photoacoustic and magnetic resonance imaging of tumors, Angew. Chem. Int. Ed. 55 (2016) 15297-15300.
- [23] R.J. Hickey, J. Koski, X. Meng, R.A. Riggleman, P. Zhang, S.-J. Park, Size-Controlled Self-Assembly of Superparamagnetic Polymersomes, ACS Nano 8 (2014) 495-502.
- [24] S. Shi, T.P. Russell, Nanoparticle assembly at liquid–liquid interfaces: From the nanoscale to mesoscale, Adv. Mater. 30 (2018) 1800714.
- [25] S.U. Pickering, Emulsions, J. Chem. Soc. Trans. 91 (1907) 2001-2021.
- [26] A.D. Dinsmore, M.F. Hsu, M.G. Nikolaides, M. Marquez, A.R. Bausch, D.A. Weitz, Colloidosomes: Selectively Permeable Capsules Composed of Colloidal Particles, Science 298 (2002) 1006-1009.
- [27] T. Bollhorst, K. Rezwan, M. Maas, Colloidal capsules: nano-and microcapsules with colloidal particle shells, Chem. Soc. Rev. 46 (2017) 2091-2126.
- [28] K.L. Thompson, M. Williams, S.P. Armes, Colloidosomes: synthesis, properties and applications, J. Colloid Interface Sci. 447 (2015) 217-228.
- [29] B. Li, C.Y. Li, Immobilizing Au nanoparticles with polymer single crystals, patterning and asymmetric functionalization, J. Am. Chem. Soc. 129 (2007) 12-13.
- [30] C.Y. Li, Polymer single crystal meets nanoparticles, J. Poly. Sci. Poly. Phys. 47 (2009) 2436-2440.
- [31] P. Geil, Polymer Single Crystals, Wiley-Interscience1963.
- [32] S.Z.D. Cheng, Phase Transitions in Polymers, the Role of Metastable States, Elsevier2008.
- [33] B. Wunderlich, Macromolecular Physics Vol. 1: Crystal Structure, Morphology, Defects, Academic Press, New York, 1973.
- [34] B. Li, B.B. Wang, R.C.M. Ferrier, C.Y. Li, Programmable Nanoparticle Assembly via Polymer Single Crystals, Macromolecules 42 (2009) 9394-9399.
- [35] B. Li, L.Y. Li, B.B. Wang, C.Y. Li, Alternating patterns on single-walled carbon nanotubes, Nature Nanotech. 4 (2009) 358-362.

- [36] B.B. Wang, B. Li, B. Zhao, C.Y. Li, Amphiphilic Janus gold nanoparticles via combining "Solid-State Grafting-to" and "Grafting-from" methods, J. Am. Chem. Soc. 130 (2008) 11594-11595.
- [37] B. Dong, T. Zhou, H. Zhang, C.Y. Li, Directed Self-Assembly of Nanoparticles for Nanomotors, ACS Nano 7 (2013) 5192-5198.
- [38] B. Dong, W. Wang, D.L. Miller, C.Y. Li, Polymer-single-crystal@nanoparticle nanosandwich for surface enhanced Raman spectroscopy, J. Mater. Chem. 22 (2012) 15526-15529.
- [39] S. Cheng, X. Li, Y. Zheng, D.M. Smith, C.Y. Li, Anisotropic ion transport in 2D polymer single crystal-based solid polymer electrolytes, Giant 2 (2020) 100021.
- [40] W. Wang, H. Qi, T. Zhou, S. Mei, L. Han, T. Higuchi, H. Jinnai, C.Y. Li, Highly robust crystalsome via directed polymer crystallization at curved liquid/liquid interface, Nat. Commun. 7 (2016) 10599.
- [41] W. Wang, M.C. Staub, T. Zhou, D.M. Smith, H. Qi, E.D. Laird, S. Cheng, C.Y. Li, Polyethylene nano crystalsomes formed at a curved liquid/liquid interface, Nanoscale 10 (2018) 268-276.
- [42] H. Qi, H. Zhou, Q. Tang, J.Y. Lee, Z. Fan, S. Kim, M.C. Staub, T. Zhou, S. Mei, L. Han, Block copolymer crystalsomes with an ultrathin shell to extend blood circulation time, Nat. Commun. 9 (2018) 3005.
- [43] H. Qi, X. Liu, D.M. Henn, S. Mei, M.C. Staub, B. Zhao, C.Y. Li, Breaking translational symmetry via polymer chain overcrowding in molecular bottlebrush crystallization, Nat. Commun. 11 (2020) 2152.
- [44] M.C. Staub, R. Li, M. Fukuto, C.Y. Li, Confined Crystal Melting in Edgeless Poly (1-lactic acid) Crystalsomes, ACS Macro Lett. 9 (2020) 1773-1778.
- [45] M.C. Staub, S. Kim, S. Yu, C.Y. Li, Porous Crystalsomes via Emulsion Crystallization and Polymer Phase Separation, ACS Macro Lett. 11 (2022) 1022-1027.
- [46] M.C. Staub, S. Yu, C.Y. Li, Poly (3-hexylthiophene)(P3HT) Crystalsomes: Tiling 1D Polymer Crystals on a Spherical Surface, Macromol. Rapid Commun. (2022) 2200529.
- [47] W. Wang, Z. Huang, E.D. Laird, S. Wang, C.Y. Li, Single-walled carbon nanotube nanoring induces polymer crystallization at liquid/liquid interface, Polymer 59 (2015) 1-9.

- [48] W. Wang, E.D. Laird, Y. Gogotsi, C.Y. Li, Bending single-walled carbon nanotubes into nanorings using a Pickering emulsion-based process, Carbon 50 (2012) 1769-1775.
- [49] B. Lotz, Crystal polymorphism and morphology of polylactides, Synthesis, Structure and Properties of Poly (lactic acid), Springer2017, pp. 273-302.
- [50] G. Liu, X. Zhang, D. Wang, Tailoring Crystallization: Towards High-Performance Poly (lactic acid), Adv. Mater. 26 (2014) 6905-6911.
- [51] G. Meng, J. Paulose, D.R. Nelson, V.N. Manoharan, Elastic Instability of a Crystal Growing on a Curved Surface, Science 343 (2014) 634-637.